Research Article | Vol. 30, No. 3 / 31 Jan 2022 / Optics Express 3620
Optics EXPRESS

Multiply-resonant second-harmonic generation using surface lattice resonances in aluminum metasurfaces

TIMO STOLT,[1] ANNA VESALA,[1] HEIKKI REKOLA,[2] PETRI KARVINEN,[2] TOMMI K. HAKALA,[2] AND MIKKO J. HUTTUNEN[1,*]

[1]Tampere University, Photonics Laboratory, Physics Unit, Tampere FI-33014, Finland
[2]Faculty of Science and Forestry, Department of Physics and Mathematics, University of Eastern Finland, FI-80101 Joensuu, Finland
[*]mikko.huttunen@tuni.fi

Abstract: Nonlinear metamaterials show potential for realizing flat nonlinear optical devices but are generally lacking in terms of achievable conversion efficiencies. Recent work has focused on enhancing nonlinear processes by utilizing high quality factor resonances, such as collective responses known as surface lattice resonances (SLRs) taking place in periodic metal nanoparticle arrays. Here, we investigate how the dispersive nature of SLRs affects the nonlinear responses of SLR-supporting metasurfaces. Particularly, we measure second-harmonic generation from aluminum nanoparticle arrays and demonstrate that by tilting the sample along two orthogonal directions, the sample can be made multiply-resonant for several pump and second-harmonic signal wavelength combinations. Characterized metasurfaces are estimated to exhibit a second-order susceptibility value of 0.40 pm/V, demonstrating aluminum as a potential material for nonlinear metasurfaces.

1. Introduction

Recent developments in miniaturized photonic devices have created a demand for nanoscale nonlinear optical components, which could be potentially addressed by a novel material class known as metamaterials [1]. They are artificial structures consisting of subwavelength building blocks, often referred to as meta-atoms. By carefully selecting the meta-atom properties, the bulk metamaterial can exhibit properties not found in natural materials, such as nanoscale phase-engineering capabilities [2,3]. Through these unique properties, metamaterials show potential for realizing novel flat photonic components, such as metalenses and meta-holograms [4,5].

In addition to their linear optical properties, also the nonlinear optical properties of metamaterials have been investigated [6–9]. For example, plasmonic metamaterials consisting of metal nanoparticles show potential for enabling efficient nonlinear processes in chip-scale devices [10,11]. The optical properties of metal nanoparticles are dominated by the collective oscillations of conduction electrons, known as localized surface plasmons [12]. They exhibit resonant behavior, known as localized surface plasmon resonances (LSPRs), which results in increased local fields near the nanoparticle surface. This local-field enhancement boosts light-matter interaction, including nonlinear processes that scale with high powers of the driving field. Therefore, utilizing LSPRs leads to dramatic enhancements of the nonlinear responses of metal nanoparticles [13–19]. Unfortunately, LSPRs are associated with considerable losses, significantly limiting their potential for nonlinear optics. However, by arranging metal nanoparticles into periodic lattices, collective responses referred to as surface lattice resonances (SLRs) emerge. They are associated with much narrower resonance linewidths and higher quality factors (Q-factors) than LSPRs [20–23]. This indicates that SLRs are also associated with remarkably stronger local-field

#449198 https://doi.org/10.1364/OE.449198
Journal © 2022 Received 1 Dec 2021; revised 11 Jan 2022; accepted 13 Jan 2022; published 19 Jan 2022

Optics EXPRESS

enhancements and smaller losses. Consequently, SLRs can be utilized to enhance the nonlinear responses of metasurfaces [24–26].

Most studies on nonlinear plasmonics have focused on singly-resonant metamaterials exhibiting a resonance either at the pump or signal wavelengths of the studied nonlinear processes [24,25,27]. However, nonlinear processes scale with the local fields at all interacting wavelengths [12,28]. Thus, for example a process of second-harmonic generation (SHG) can be enhanced by utilizing multiply-resonant materials, where the resonance enhancement occurs both at the signal and pump wavelengths [29–34]. Furthermore, recent numerical work suggests that multiply-resonant operation based on SLRs could dramatically increase nonlinear responses of plasmonic metasurfaces [35].

Here, we experimentally demonstrate multiply-resonant enhancement of SHG in SLR-exhibiting metasurfaces consisting of V-shaped aluminum (Al) nanoparticles. We achieve multiply-resonant operation by tilting the investigated metasurfaces and by utilizing the dispersion of SLRs. The multiply-resonant conditions are fulfilled at several different wavelengths, demonstrating the tunability of SLR-enhanced responses. The measured SH signals correspond to nonlinear susceptibility tensor values of 0.40 pm/V, which is of the same order-of-magnitude as the typical values for traditional nonlinear materials [28].

2. Theory

2.1. Surface lattice resonances

The optical properties of metals are governed by the collective oscillations of conduction electrons known as plasmons [12]. At resonant conditions, the strength of light–matter interaction increases, resulting in dramatic changes of, e.g., reflectivity and absorbance of the bulk metal. In the case of metal nanoparticles, plasmons are restricted to the particle surface [36]. Therefore, in resonant conditions, incident light is coupled to the local plasmon modes resulting in increased local fields near the nanoparticle surface. This phenomenon is known as LSPR, and it is widely used in many applications of plasmonic metamaterials [37–39]. LSPRs are associated with relatively broad linewidths and therefore low Q-factors ($Q \sim 10$), which indicate extremely short resonance lifetimes but, on the other hand, considerable losses and relatively low local-field enhancements. The low field enhancement can be compensated by using optically dense plasmonic structures and intense pulsed laser sources. Unfortunately, the subsequent strong absorption decrease damage thresholds of the plasmonic structures, significantly limiting the usable input power and thus the strength of the nonlinear responses of plasmonic metamaterials.

A viable approach to decrease losses and increase the interaction strength in plasmonic metamaterials is to utilize SLRs. They are propagating surface modes resulting from radiative coupling of localized surface plasmons in a periodic grating of nanoparticles. They are associated with remarkably high Q-factors ($Q \sim 1000$) [23], indicating significantly higher local-field enhancements than the ones associated with LSPRs. Because SLRs result from diffractive properties of the metasurface, their spectral locations are related to the Rayleigh anomalies (RAs) according to [40,41]

$$\lambda_{l,m}(\theta, \phi) = -A_{l,m}(\theta, \phi) + \sqrt{A_{l,m}^2(\theta, \phi) - B_{l,m}(\theta)}, \tag{1}$$

where l and m are the diffraction orders along the Cartesian coordinates of the grating, θ is the incidence angle in the incidence plane, and ϕ is the azimuthal angle that defines the orientation of the incidence plane with respect to the Cartesian coordinates. For a rectangular metasurface with lattice constants p_x and p_y along the surface Cartesian coordinates (see Fig. 1), the variables $A_{l,m}(\theta, \phi)$ and $B_{l,m}(\theta)$ are given by

$$A_{l,m}(\theta, \phi) = \frac{\sin\theta}{(l/p_x)^2 + (m/p_y)^2} \left(\frac{l \sin\phi}{p_x} + \frac{m \cos\phi}{p_y} \right), \tag{2}$$

Optics EXPRESS

$$B_{l,m}(\theta) = \frac{\sin^2\theta - n^2}{(l/p_x)^2 + (m/p_y)^2}, \tag{3}$$

where n is the refractive index of the surrounding material.

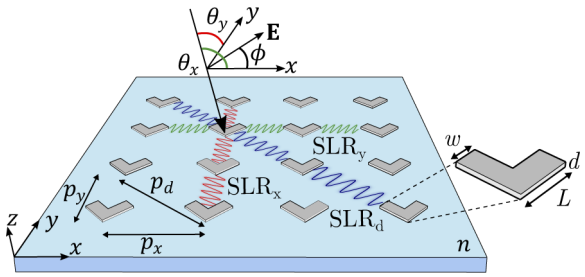

Fig. 1. Surface lattice resonance (SLR) modes propagate along the metasurface. Their spectral location depends on numerous factors: incidence angle (θ), azimuthal angle (ϕ), refractive index (n), and lattice constants p_x, p_y, and p_d. For y-polarized light ($\phi = 90°$), parallel SLRs (green waves) depend on θ_x and p_x, and for x-polarized light ($\phi = 0°$), the emerging SLRs depend on and θ_y and p_y (red waves). The diagonal SLRs (blue waves) occur for both polarizations. In this work, we consider metasurfaces consisting of V-shaped nanoparticles with arm length L, arm width w, and thickness d. These parameters dictate localized surface plasmon resonances of individual nanoparticles, which also impact the SLR formation.

In this work, we focus on in-plane SLRs that occur when the polarization of the incident light and the induced dipoles in the nanoparticles are parallel to the metasurface, i.e., when the incident light is TE polarized [42]. These SLR modes propagate along the metasurface in the directions that are not parallel with incident polarization. The most obvious option for nanoparticles to couple is along the direction that is perpendicular to the incident polarization, resulting in surface modes we name as parallel SLR.

Here, we are interested in first-order parallel SLRs for light polarized along either the x- or y-axis of the rectangular metasurface. For x-polarized light ($\phi = 0°$), the SLR wavelength depends on p_y and the incidence angle θ_y on the yz-plane (see Fig. 1) as given by

$$\lambda_x(\theta_y) = \lambda_{0,\pm1}(\theta_y) = p_y\left(n \mp \sin\theta_y\right). \tag{4}$$

For y-polarized light ($\phi = 90°$), a similar condition is found to be

$$\lambda_y(\theta_x) = \lambda_{\pm1,0}(\theta_x) = p_x\left(n \mp \sin\theta_x\right), \tag{5}$$

where θ_x is the incidence angle along the xz-plane with respect to the metasurface normal.

Plasmon modes in a rectangular lattice can couple also along the diagonal of the lattice unit cell, resulting in diagonal SLRs (blue waves in Fig. 1). At normal incidence ($\theta_x = \theta_y = 0°$), the diagonal SLRs occur at the same wavelength for both incident polarizations, which for first-order SLRs is given by

$$\lambda_d = n\frac{p_x p_y}{p_d}, \tag{6}$$

where $p_d = \sqrt{p_x^2 + p_y^2}$ is the diagonal of the metasurface unit cell.

Overall, the spectral location of the SLR depends on the polarization of the interacting wave, the lattice constants p_x and p_y, the refractive index of the surrounding material n, and the incidence angles θ_x and θ_y, providing us multiple parameters to control the occurrence of SLRs.

Optics EXPRESS

2.2. Second-harmonic generation in multiply-resonant structures

The SH responses of metamaterials depend on the local fields $E_{\mathrm{loc}}(\omega)$ and $E_{\mathrm{loc}}(2\omega)$, oscillating at the fundamental and SH frequency, respectively [12,28]. Therefore, we can write for far-field SH emission $E_{\mathrm{nl}}(2\omega)$ that

$$E_{\mathrm{nl}}(2\omega) \propto \chi^{(2)} E_{\mathrm{loc}}(2\omega) E^2_{\mathrm{loc}}(\omega), \tag{7}$$

where $\chi^{(2)}$ is the effective nonlinear susceptibility of the metasurface.

The local electric fields in Eq. (7) can be enhanced by utilizing metasurface responses, such as LSPRs and SLRs, at the interacting wavelengths. Most works have considered singly-resonant metasurfaces that exhibit resonances at either the signal or more commonly at the fundamental wavelength [24,43]. However, the nonlinear responses can be further enhanced by utilizing multiply-resonant metasurfaces that exhibit resonances at both interacting wavelengths. For example, Celebrano et al. designed metasurfaces consisting of gold nanoparticles exhibiting LSPRs to enhance SHG [30]. In this work, we extend the approach to metasurfaces based on SLRs with clear benefits. As mentioned before, SLRs are very dependent on the polarization state and propagation direction of the interacting laser fields. Therefore, we design our metasurfaces for type-I SHG, where both fundamental fields have the same polarization state k, while the emitted signal field is associated with a different polarization state j. For this process, we can rewrite Eq. (7) as follows:

$$E_{nl}(\mathbf{k}_2, 2\omega) \propto \chi^{(2)}_{jkk} E_{\mathrm{loc},j}(\mathbf{k}_2, 2\omega) E^2_{\mathrm{loc},k}(\mathbf{k}_1, \omega), \tag{8}$$

where $\mathbf{k}_1$ and $\mathbf{k}_2$ are the wavevectors of fundamental and SH beams, respectively, and $\chi^{(2)}_{jkk}$ is the corresponding effective nonlinear susceptibility tensor component.

3. Methods

3.1. Sample fabrication

For this work, we fabricated Al nanoparticle arrays with a total area of 300×300 μm. The structures were fabricated on a pre-cleaned microscope slide (Schott Nexterion, D263T glass). A 200 nm layer of PMMA-resist (MicroChem, 950k) was spin-coated on top and baked on a hot plate at 180°C for 180 s. A 10 nm layer of Al was evaporated on the resist to act as a conductive layer for electron beam lithography.

The patterning was done using a Raith EBPG 5000+ 100 kV electron beam lithography system. After patterning the Al layer was removed using a 1% sodium hydroxide solution. The resist was then developed using a 1:3 mixture of methyl isobutyl ketone and isopropanol (IPA) for 15 s, followed by a 30 s immersion in IPA. The sample was dried with nitrogen and placed in an electron beam evaporator for depositing 30 nm of Al. Finally, a liftoff process was performed by soaking the sample in acetone overnight and gently washing the surface with more acetone using a syringe. This removes the resist and excess metal on top of it, leaving only the nanoparticles on the glass substrate. The sample was then rinsed with IPA and dried with nitrogen.

Before the measurements, we covered the metasurface with index-matching oil and an anti-reflection (AR) coated coverslip with the AR wavelength band at 1000–1300 nm. This way, the nanoparticles were assured to have a homogeneous surrounding, and we avoided any Fabry–Pérot resonances resulting from multiple reflections from different interfaces present in the fabricated devices.

3.2. Experiments

In this work, we characterized both linear and nonlinear optical properties of our metasurfaces using two different experimental setups. Here, only short descriptions are given while further details are described in Supplement 1.

Optics EXPRESS

In order to characterize the linear optical properties of our samples, especially the properties of the occurring SLRs, we measured transmission spectra of our samples (see Figs. 2, 3(a)–(b), and 4(a)–(b)) Here, we used a broadband halogen lamp, a linear polarizer, and spectrometers to locate SLRs. We placed the sample on a goniometer on a rotational stage, which was connected to a 3-axis translational stage. This enabled continuous control over sample position and orientation, especially with respect to angles θ_y and θ_x. By measuring the transmission spectra at different angles, we extracted the dispersion relation graphs shown in Figs. 3(a)–(b) and 4(a)–(b).

In our nonlinear experiments, we used an optical parametric oscillator (1000–1300 nm) pumped with a titanium sapphire femtosecond laser (800 nm, repetition rate 82 MHz, pulse duration 200 fs) as a tunable laser source. We set our laser power to 75 mW using a combination of a linear polarizer, an achromatic half-wave plate and a reference diode. The laser beam was then weakly focused on the sample using an achromatic lens (f = 500 mm), resulting in estimated beam diameter ($1/e^2$ of maximum intensity) of 75 μm and peak intensity of 115 MW/cm^2 at the sample plane. Similar to the transmission experiments, we placed the sample on a stage that allows fine-tuning of sample position and accurate control of θ_y and θ_x. In this setup, the rotation stage was motorized allowing continuous incidence angle scans. The generated SH signal was collected with a photo-multiplier tube. By repeating angle scans for different pump wavelengths, we acquired the (λ, θ)-graphs for the SHG emission from studied metasurfaces, shown in Figs. 3(c) and 4(c).

4. Design and results

Our metasurfaces consisted of V-shaped Al nanoparticles with arm length L = 100 nm, arm width w = 70 nm, and thickness d = 30 nm (see Fig. 1). The nanoparticles were fabricated on a glass substrate (refractive index n = 1.51) [See the Sample Fabrication section for details]. The nanoparticles were arranged in rectangular lattices with lattice constants p_y and p_x along and orthogonal to the nanoparticle symmetry axis (y-axis), respectively (see Fig. 1). In such configuration, the metasurface has the following non-zero second-order susceptibility tensor components $\chi^{(2)}_{yyy}$, $\chi^{(2)}_{yxx}$, and $\chi^{(2)}_{xxy} = \chi^{(2)}_{xyx}$ [44]. Additionally, under illumination of x- or y-polarized

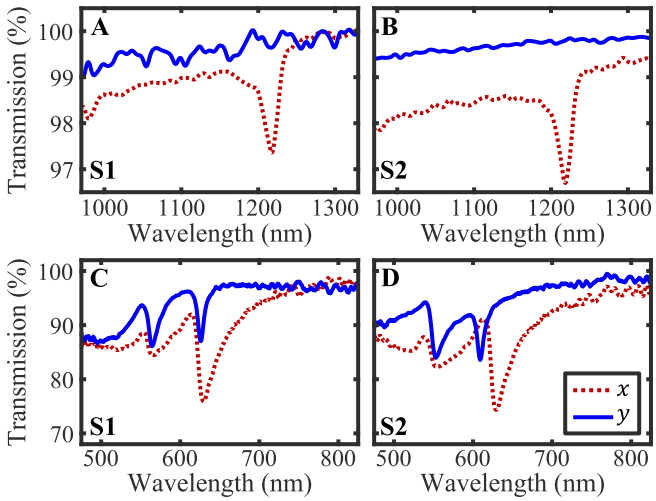

Fig. 2. Measured tranmsission spectra for the studied periodic aluminum metasurfaces (see Fig. 1). (a)–(b) The two studied samples, S1 and S2, had p_y = 813 nm, resulting in first-order SLRs at 1220 nm for x-polarized light (dotted red lines). (c)–(d) S1 (S2) has p_x = 410 nm (398 nm), resulting in first-order SLR at 626 nm (609 nm) for y-polarized light (blue solid lines). Furthermore, S1 (S2) exhibit diagonal SLRs at 560 nm (546 nm).

Optics EXPRESS

light, local field hotspots form in the tips of the V-shaped nanoparticles [45]. We note that similar array configurations have been shown to result in SLRs at different spectral regions [46].

Here, we studied two metasurfaces composed of identical nanoparticles but varying in their array periodicities. For sample S1, the periodicities were $p_x = 410$ nm and $p_y = 813$, and for sample S2, $p_x = 398$ nm and $p_y = 813$ nm. Since both samples are composed of identical nanoparticles, they both exhibit LSPRs centered at 475 nm and 550 nm for y- and x-polarized light, respectively (see Supplement 1 for more information). The samples also have the same $p_y = 813$ nm, and therefore, at normal incidence, they exhibit the first-order SLR for x-polarized light at $\lambda_x(0°) = 1220$ nm (see Fig. 2(a)). The two samples differ in p_x, and therefore, also in location of parallel SLRs for y-polarized light ($\lambda_y(\theta_x)$) and diagonal SLRs for both polarizations (λ_d). At normal incidence, these SLRs occur at $\lambda_y(0°) = 626$ nm (609 nm) and $\lambda_d = 560$ nm (546 nm) for the sample S1 (S2).

Our metasurfaces were designed for the multiply-resonant enhancement of SHG corresponding to $\chi^{(2)}_{yxx}$, i.e., to the process with x-polarized pump and y-polarized SH signal. The multiply-resonant operation is therefore enabled for SHG processes where the pump is coupled to the x-polarized SLR and the signal to the y-polarized SLR, either parallel or diagonal. Thus, we can write the condition for multiply-resonant operation with resonance wavelengths $\lambda_x(\theta_y)$ and $\lambda_y(\theta_x)$ to be

$$\lambda_x(\theta_y) = 2\lambda_y(\theta_x), \tag{9}$$

where θ_y and θ_x emphasize the fact that we modify the SLR wavelengths by rotating the sample accordingly. This way, the experiment corresponds to a situation where the sample is illuminated at an angle θ_y and the SH signal is collected at an angle θ_x.

For sample S1, the multiply-resonant condition of Eq. (9) is not fulfilled at normal incidence, but can be achieved by utilizing the dispersion of the occurring SLRs (see Figs. 3(a) and 3(b)). Here, we selected $\theta_y = 3°$ for which S1 exhibit x-polarized SLRs at 1176 nm and 1250 nm (red circle in Fig. 3(a)). Then, we utilize the dispersion of y-polarized SLRs to fulfill the multiply-resonant condition at three different conditions (dashed circles in Fig. 3(b)). For the pump wavelength of 1176 nm, the multiply-resonant condition is fulfilled at $\theta_x = \pm 5°$, where parallel SLRs (green dots) and diagonal SLRs (blue dots) overlap at 590 nm. For the pump wavelength of 1250 nm, the multiply-resonant condition is fulfilled conveniently at $\theta_x = 0°$, where the fundamental y-polarized SLR occurs at 626 nm. These locations of multiply-resonant operation are marked in Figs. 3(a) and 3(b) with dashed circles.

To demonstrate multiply-resonant operation using the angle–wavelength combinations mentioned above, we set $\theta_y = 3°$ and measured the SHG (θ_x, λ) -spectrum corresponding to $\chi^{(2)}_{yxx}$, i.e., to the SHG process with x-polarized pump and y-polarized signal (see Fig. 3(c)). The SH emission pattern follows the dispersion of y-polarized SLRs, and the signal reaches its maximum when multiple SLRs occur at interacting wavelengths (green and blue circles). At these locations, the SH emission is 8-fold, when compared against the off-resonance signal. The maximum emission power is 5.7 fW, which corresponds to a conversion efficiency of 7.6×10^{-14}. By using the method presented by Herman et al. [47,48], we estimate a value $\chi^{(2)}_{yxx} = 0.36$ pm/V for the sample S1 (see Supplement 1 for calculation details).

However, the maximum SH signal is achieved, when diagonal and parallel SLRs overlap at 590 nm. This overlap results in stronger resonance than the separate SLRs. Additionally, the two SLRs near the pump wavelengths 1176 nm and 1250 nm are considerably weak, when compared against, e.g., the normal-incidence SLR at 1220 nm. Thus, we cannot confidently confirm that the strong signals observed with the pump wavelength of 1176 nm results from multiply-resonant operation or simply from overlapping SLRs at the signal wavelength. To undoubtedly demonstrate multiply-resonant enhancement, we measured the SH response from the sample S2.

For the sample S2, the multiply-resonant condition in Eq. (9) is fulfilled at normal incidence ($\theta_y = 0°$ and $\theta_x = 0°$) for the pump wavelength of 1220 nm (red circle in Fig. 4(a) and green circle

Optics EXPRESS

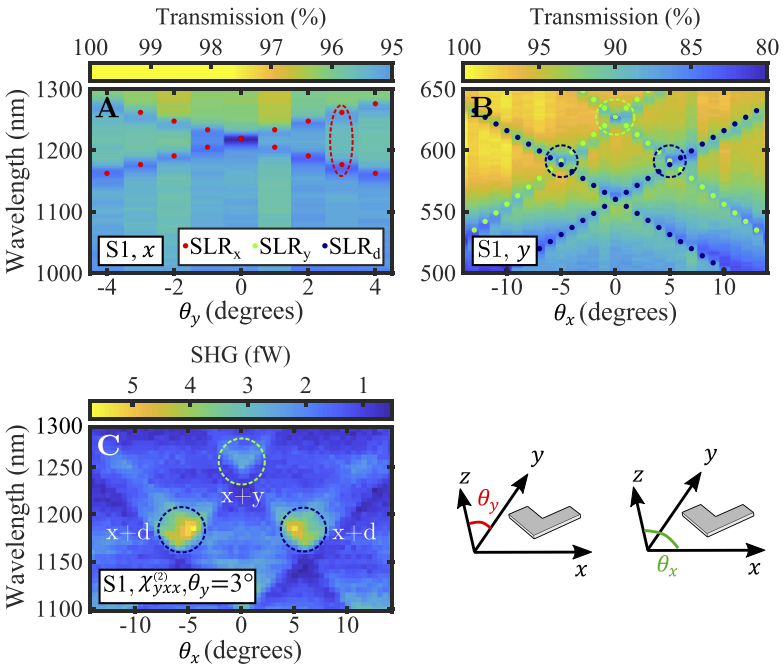

Fig. 3. The dispersion graphs of transmission for (a) x- and (b) y-polarized incident light. (c) The dispersion graph of SHG emission for the sample S1, with x-polarized pump and y-polarized SHG signal. (a)–(b) At normal incidence ($\theta_y = \theta_x = 0°$), sample S1 exhibits first-order parallel SLRs at 1220 nm and 626 nm for x-polarized (red dots) and y-polarized (green dots) light, respectively. Additionally, diagonal SLRs (blue dots) occur at 560 nm for normal incidence illumination. By tilting the sample, the SLRs shift from their normal-incidence values. (c) SLRs occurring near the pump and signal wavelengths impact the SHG associated with $\chi^{(2)}_{yxx}$. By setting $\theta_y = 3°$ (dashed circle in a) and tilting sample with respect to x-axis (θ_x), the SH emission is enhanced with three different wavelength–angle combinations (dashed circles in b). At $\theta_x = 0°$, the parallel SLRs for x- and y-polarized light enhance SHG at 1250 nm (green circle). At $\theta_x = \pm 5°$, parallel and diagonal SLRs for y-polarized light overlap at 590 nm, and parallel SLR for x-polarization occurs at 1176 nm. Combined, these SLRs enhance SHG near 1180 nm (blue circles).

in (b)). By rotating the sample along the x-axis, i.e., by changing θ_x, the diagonal SLRs (red dots) shift from $\lambda_d = 546$ nm. At $\theta_x = \pm 11°$ $\lambda_d = 610$ nm and the multiply-resonant condition is again fulfilled (blue circles in Fig. 4(b)).

To confirm the multiply-resonant operation, we measured the SHG (θ_x, λ)-spectrum by setting $\theta_y = 0°$ and scanning over a wavelength range of 1000–1300 nm and an angle range (θ_x) from $-15°$ to $15°$ (see Fig. 4(c)). From the SH emission pattern it is clear, that the x-polarized SLR enhances the nonlinear response, as there is significant signal at all values of θ_x at the pump wavelength of 1220 nm. Other parts of the SH emission pattern again follows the dispersion of y-polarized SLRs and reaches its maximum at multiply-resonant conditions, i.e., at 1220 nm when $\theta_x = [0°, \pm 11°]$ (marked with green and blue circles). Now, the multiply-resonant enhancement results in 10-fold enhancement and the maximum emission power of 5.8 fW. The measured signal therefore corresponds to conversion efficiency 7.7×10^{-14} and $\chi^{(2)}_{yxx} = 0.40$ pm/V.

For sample S2, the impact of multiply-resonant operation is more evident. The SH emission with the pump wavelength of 1220 nm is visibly enhanced at all angles θ_x, demonstrating the impact of the SLR at the pump wavelength. More importantly, the signal reaches the maximum

Optics EXPRESS

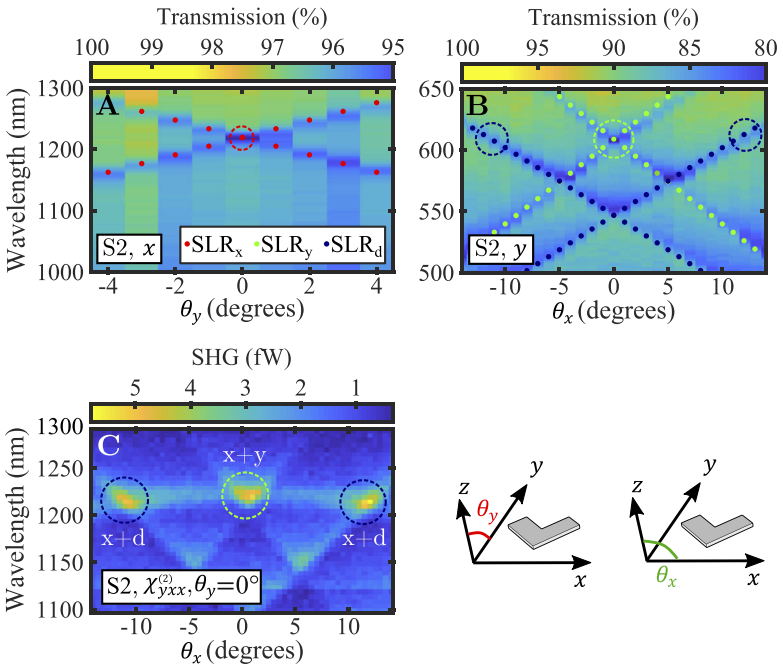

Fig. 4. The dispersion graphs of transmission for (a) x- and (b) y-polarized incident light for the sample S2. (c) The dispersion graph of SHG emission for the sample S2, with x-polarized pump and y-polarized SHG signal. (a)–(b) At normal incidence, sample S2 exhibits first-order parallel SLRs at 1220 nm and 609 nm for x-polarized (red dots) and y-polarized (green dots) light, respectively. The sample exhibits also diagonal SLRs (blue dots) at 546 nm. Tilting sample along y-axis (θ_y) and x-axis (θ_x) will shift x- and y-polarized SLRs from their normal incidence values. By setting $\theta_y = 0°$, the multiply-resonant condition for SHG associated with $\chi^{(2)}_{yxx}$ ($\lambda_x = 2\lambda_y$) is fulfilled when $\theta_x = [0°, \pm 11°]$ (dashed circles). (c) SLRs enhance the second-harmonic emission and the maximum value is achieved at the multiply-resonant condition. With the incident angle set to $\theta_y = 0°$, this occurs at the pump wavelength 1220 nm with three different emission angles θ_x. First, at $\theta_x = 0°$ (green circle), the multiply-resonant condition is fulfilled with parallel SLRs. At $\theta_x = \pm 11$ (blue circles), S2 exhibit diagonal SLRs at 610 nm, therefore fulfilling the multiply-resonant condition.

level only, when the multiply-resonant condition is fulfilled with parallel and diagonal SLRs occurring at 610 nm, marked in Fig. 4(c) with green and blue circles, respectively.

5. Discussion

Our results demonstrate two things. First, only few studies have characterized the nonlinear properties of Al nanostructures [49,50]. This is due to the fact that Al spontaneously forms oxides (Al_2O_3), which impacts the plasmonic properties of the Al nanoparticles [51]. Therefore, many researchers prefer more stable plasmonic nanostructures, such as gold and silver nanoparticles [52]. However, our work utilizes the diffractive properties of plasmonic metasurfaces, which are less sensitive to the changes in LSPRs induced by the oxidation of Al nanoparticles. Furthermore, the use of gold or silver nanoparticles would have shifted LSPRs to longer wavelengths, i.e., to the SHG wavelength range of our studies. Thus, we would not have achieved multiply-resonant operation by utilzing only SLRs if gold or silver nanoparticles were used.

Optics EXPRESS

Second, our results demonstrate the multiply-resonant enhancement of SHG by utilizing only SLRs. Other works have either utilized only LSPRs or singly-resonant structures that exhibit SLRs near either the pump or signal wavelengths [41]. Unfortunately, our results demonstrate only 10-fold on-and-off-resonance enhancement and SH signal levels of 5 fW, which are significantly lower than the corresponding values acquired with singly-resonant SLR-based structures [24,25]. A major reason for this difference is the fact that our samples exhibited relatively weak and low-Q SLRs (extinction $\leq$ 5% and $Q \approx 60$) at the pump wavelength. Thus, the SLR-induced field enhancements were also relatively weak. These points originated mostly from the fact that the nanoparticles themselves were relatively small when compared against the lattice constant p_y, which weakened the inter-particle coupling. However, our OPO restricted the investigation to pump wavelengths of 1000–1300 nm and signal wavelengths of 500–650 nm. Having larger nanoparticles would have shifted the LSPRs to the desired signal wavelength range, preventing us from using only SLRs to realize multiply-resonant operation. Furthermore, highly transparent structures could prove to be useful in future investigations. For example, multiple such structures could be stacked on top of each other to achieve phase-matched SHG boosting the overall nonlinear signal [53].

Another factor that might explain the weakness of the measured SHG signals is the possible poor spatial overlap between local fields induced by different SLR modes. We note that such mode-overlap calculations have been already performed for very similar periodic metasurfaces elsewhere [54], where the use of oblique angles of incidence did not dramatically affect the estimated SHG signals. Therefore, we do not think this reason is the most probable one to explain the weakness of the SHG signal. Unfortunately, due to our restricted computational capabilities, we did not have the resources to repeat such calculations for the general 2D situation we have in this work experimentally investigated. We also note, that due to the non-local nature of SLRs, the conventional susceptibility formalism may not anymore be adequate if a broad range of angles of incidence would be used. In such case, it would seem preferable to estimate the nonlinear responses by performing mode-overlap calculations [54]. Alternatively, it might be possible to estimate angle-dependent nonlinear responses by using an approach based on the nonlinear discrete-dipole approximation [55]. Although the latter approach approximates individual nanoparticles as point-like scatterers, and does not therefore permit mode-overlap calculations, the approach is computational less intensive than approaches based on full-wave simulations.

Despite the relatively low signal levels, our results demonstrate how SHG can be modified by utilizing the dispersion of SLRs. As is shown in Figs. 3 and 4, SLRs near both pump and signal wavelengths enhance the SH response, which reaches its maximum at the multiply-resonant conditions. By tilting the sample accordingly, we can change the multiply-resonant wavelength, i.e., tune the wavelength of the maximum SH response. Such post-fabrication tunability could prove useful for realizing other nonlinear processes in resonant metasurfaces, such as sum-frequency generation, difference-frequency generation, and third-harmonic generation [35]. Demonstrating these processes could pave the path towards flat and tunable laser sources with the operation band ranging from the ultraviolet to the terahertz (THz) region of the electromagnetic spectrum.

6. Conclusion

In summary, we demonstrate multiply-resonant enhancement of second-harmonic generation from Al metasurfaces. The achieved signal levels correspond to the nonlinear susceptibility tensor component value of 0.40 pm/V, which is the same order-of-magnitude as the susceptibility values of conventional nonlinear optical materials, demonstrating the potential of Al metasurfaces for nonlinear optics. Here, we achieve the multiply-resonant enhancement by utilizing collective responses of periodic metal nanoparticle arrays known as surface lattice resonances. Due to

Optics EXPRESS

the dispersion of surface lattice resonances, we can control the multiply-resonant enhancement by tilting the sample. As a result, we achieve multiply-resonant enhancement with several different combinations of signal wavelength, incidence angle, and signal emission angle, therefore demonstrating tunable second-harmonic generation. Our methods show promise for realizing other nonlinear processes in plasmonic metasurfaces. Such structures could pave the path towards flat and tunable nonlinear devices.

Funding. Academy of Finland (308596, 320165, 320166, 322002); Jenny ja Antti Wihurin Rahasto (Doctoral study grant).

Acknowledgements. Authors acknowledge Jarno Reuna for providing anti-reflection coatings.

Disclosures. Authors declare no conflicts of interest.

Data availability. Data underlying the results presented in this paper are not publicly available at this time but may be obtained from the authors upon reasonable request.

Supplemental document. See Supplement 1 for supporting content.

References

1. C. M. Soukoulis and M. Wegener, "Past achievements and future challenges in the development of three-dimensional photonic metamaterials," Nat. Photonics **5**(9), 523–530 (2011).
2. P. Genevet, F. Capasso, F. Aieta, M. Khorasaninejad, and R. Devlin, "Recent advances in planar optics: from plasmonic to dielectric metasurfaces," Optica **4**(1), 139 (2017).
3. S. Chen, Z. Li, Y. Zhang, H. Cheng, and J. Tian, "Phase Manipulation of Electromagnetic Waves with Metasurfaces and Its Applications in Nanophotonics," Adv. Opt. Mater. **6**(13), 1800104 (2018).
4. F. Aieta, M. A. Kats, P. Genevet, and F. Capasso, "Achromatic metasurfaces by dispersive phase compensation," Science **347**(6228), 1342–1345 (2015).
5. M. Khorasaninejad, A. Ambrosio, P. Kanhaiya, and F. Capasso, "Broadband and chiral binary dielectric meta-holograms," Sci. Adv. **2**(5), 1 (2016).
6. A. D. Boardman, V. V. Grimalsky, Y. S. Kivshar, S. V. Koshevaya, M. Lapine, N. M. Litchinitser, V. N. Malnev, M. Noginov, Y. G. Rapoport, and V. M. Shalaev, "Active and tunable metamaterials," Laser Photonics Rev. **5**(2), 287–307 (2011).
7. S. Keren-Zur, L. Michaeli, H. Suchowski, and T. Ellenbogen, "Shaping light with nonlinear metasurfaces," Adv. Opt. Photonics **10**(1), 309 (2018).
8. A. Krasnok, M. Tymchenko, and A. Alù, "Nonlinear metasurfaces: a paradigm shift in nonlinear optics," Mater. Today **21**(1), 8–21 (2018).
9. B. Sain, C. Meier, and T. Zentgraf, "Nonlinear optics in all-dielectric nanoantennas and metasurfaces: a review," Adv. Photonics **1**(2), 024002 (2019).
10. M. Kauranen and A. V. Zayats, "Nonlinear plasmonics," Nat. Photonics **6**(11), 737–748 (2012).
11. J. Lee, M. Tymchenko, C. Argyropoulos, P. Y. Chen, F. Lu, F. Demmerle, G. Boehm, M. C. Amann, A. Alù, and M. A. Belkin, "Giant nonlinear response from plasmonic metasurfaces coupled to intersubband transitions," Nature **511**(7507), 65–69 (2014).
12. S. A. Maier, *Plasmonics: fundamentals and applications* (Springer Science & Business Media, 2007).
13. M. W. Klein, C. Enkrich, M. Wegener, and S. Linden, "Second-harmonic generation from magnetic metamaterials," Science **313**(5786), 502–504 (2006).
14. M. Lapine, I. V. Shadrivov, and Y. S. Kivshar, "Colloquium: Nonlinear metamaterials," Rev. Mod. Phys. **86**(3), 1093–1123 (2014).
15. J. Butet, P. F. Brevet, and O. J. Martin, "Optical Second Harmonic Generation in Plasmonic Nanostructures: From Fundamental Principles to Advanced Applications," ACS Nano **9**(11), 10545–10562 (2015).
16. M. S. Nezami and R. Gordon, "Localized and propagating surface plasmon resonances in aperture-based third harmonic generation," Opt. Express **23**(25), 32006 (2015).
17. G. Li, S. Zhang, and T. Zentgraf, "Nonlinear photonic metasurfaces," Nat. Rev. Mater. **2**(5), 17010 (2017).
18. E. Rahimi and R. Gordon, "Nonlinear Plasmonic Metasurfaces," Adv. Opt. Mater. **6**(18), 1800274 (2018).
19. M. J. Huttunen, R. Czaplicki, and M. Kauranen, "Nonlinear plasmonic metasurfaces," J. Nonlinear Opt. Phys. Mater. **28**(01), 1950001 (2019).
20. W. Wang, M. Ramezani, A. I. Väkeväinen, P. Törmä, J. G. Rivas, and T. W. Odom, "The rich photonic world of plasmonic nanoparticle arrays," Mater. Today **21**(3), 303–314 (2018).
21. V. G. Kravets, A. V. Kabashin, W. L. Barnes, and A. N. Grigorenko, "Plasmonic Surface Lattice Resonances: A Review of Properties and Applications," Chem. Rev. **118**(12), 5912–5951 (2018).
22. A. D. Utyushev, V. I. Zakomirnyi, and I. L. Rasskazov, "Collective lattice resonances: Plasmonics and beyond," Rev. Phys. **6**, 100051 (2021).

Optics EXPRESS

23. M. S. Bin-Alam, O. Reshef, Y. Mamchur, M. Z. Alam, G. Carlow, J. Upham, B. T. Sullivan, J.-M. Ménard, M. J. Huttunen, R. W. Boyd, and K. Dolgaleva, "Ultra-high-q resonances in plasmonic metasurfaces," Nat. Commun. **12**(1), 974 (2021).
24. L. Michaeli, S. Keren-Zur, O. Avayu, H. Suchowski, and T. Ellenbogen, "Nonlinear surface lattice resonance in plasmonic nanoparticle arrays," Phys. Rev. Lett. **118**(24), 243904 (2017).
25. D. C. Hooper, C. Kuppe, D. Wang, W. Wang, J. Guan, T. W. Odom, and V. K. Valev, "Second harmonic spectroscopy of surface lattice resonances," Nano Lett. **19**(1), 165–172 (2019).
26. A. Han, C. Dineen, V. E. Babicheva, and J. V. Moloney, "Second harmonic generation in metasurfaces with multipole resonant coupling," Nanophotonics **9**(11), 3545–3556 (2020).
27. B. Shen, L. Liu, Y. Li, S. Ren, J. Yan, R. Hu, and J. Qu, "Nonlinear spectral-imaging study of second- and third-harmonic enhancements by surface-lattice resonances," Adv. Opt. Mater. **8**(8), 1901981 (2020).
28. R. W. Boyd, *Nonlinear optics* (Academic Press, San Diego, 2020), 4th ed.
29. K. Thyagarajan, S. Rivier, A. Lovera, and O. J. Martin, "Enhanced second-harmonic generation from double resonant plasmonic antennae," Opt. Express **20**(12), 12860–12865 (2012).
30. M. Celebrano, X. Wu, M. Baselli, S. Großmann, P. Biagioni, A. Locatelli, C. De Angelis, G. Cerullo, R. Osellame, B. Hecht, L. Duò, F. Ciccacci, and M. Finazzi, "Mode matching in multiresonant plasmonic nanoantennas for enhanced second harmonic generation," Nat. Nanotechnol. **10**(5), 412–417 (2015).
31. S. D. Gennaro, M. Rahmani, V. Giannini, H. Aouani, T. P. Sidiropoulos, M. Navarro-Cía, S. A. Maier, and R. F. Oulton, "The Interplay of Symmetry and Scattering Phase in Second Harmonic Generation from Gold Nanoantennas," Nano Lett. **16**(8), 5278–5285 (2016).
32. K. Y. Yang, J. Butet, C. Yan, G. D. Bernasconi, and O. J. Martin, "Enhancement mechanisms of the second harmonic generation from double resonant aluminum nanostructures," ACS Photonics **4**(6), 1522–1530 (2017).
33. M. Minkov, D. Gerace, and S. Fan, "Doubly resonant $\chi^{(2)}$ nonlinear photonic crystal cavity based on a bound state in the continuum," Optica **6**(8), 1039 (2019).
34. L. Soun, B. Fix, H. E. Ouazzani, S. Héron, N. Bardou, C. Dupuis, S. Derelle, J. Jaeck, R. Haïdar, and P. Bouchon, "Experimental demonstration of second-harmonic generation in high χ^2 metasurfaces," Opt. Lett. **46**(6), 1466 (2021).
35. M. J. Huttunen, O. Reshef, T. Stolt, K. Dolgaleva, R. W. Boyd, and M. Kauranen, "Efficient nonlinear metasurfaces by using multiresonant high-Q plasmonic arrays," J. Opt. Soc. Am. B **36**(7), E30–E35 (2019).
36. K. Yao and Y. Liu, "Plasmonic metamaterials," Nanotechnol. Rev. **3**(2), 177–210 (2014).
37. E. Petryayeva and U. J. Krull, "Localized surface plasmon resonance: Nanostructures, bioassays and biosensing-a review," Anal. Chim. Acta **706**(1), 8–24 (2011).
38. X. Gu, T. Qiu, W. Zhang, and P. K. Chu, "Light-emitting diodes enhanced by localized surface plasmon resonance," Nanoscale Res. Lett. **6**(1), 199 (2011).
39. P. F. Gao, Y. F. Li, and C. Z. Huang, "Localized surface plasmon resonance scattering imaging and spectroscopy for real-time reaction monitoring," Appl. Spectrosc. Rev. **54**(3), 237–249 (2019).
40. T. W. Maß and T. Taubner, "Incident angle-tuning of infrared antenna array resonances for molecular sensing," ACS Photonics **2**(10), 1498–1504 (2015).
41. R. Czaplicki, A. Kiviniemi, J. Laukkanen, J. Lehtolahti, M. Kuittinen, and M. Kauranen, "Surface lattice resonances in second-harmonic generation from metasurfaces," Opt. Lett. **41**(12), 2684–2687 (2016).
42. K. Volk, J. P. Fitzgerald, and M. Karg, "In-plane surface lattice and higher order resonances in self-assembled plasmonic monolayers: From substrate-supported to free-standing thin films," ACS Appl. Mater. Interfaces **11**(17), 16096–16106 (2019).
43. R. Czaplicki, A. Kiviniemi, M. J. Huttunen, X. Zang, T. Stolt, I. Vartiainen, J. Butet, M. Kuittinen, O. J. F. Martin, and M. Kauranen, "Less is more – enhancement of second-harmonic generation from metasurfaces by reduced nanoparticle density," Nano Lett. **18**(12), 7709–7714 (2018).
44. R. Czaplicki, J. Mäkitalo, R. Siikanen, H. Husu, J. Lehtolahti, M. Kuittinen, and M. Kauranen, "Second-harmonic generation from metal nanoparticles: Resonance enhancement versus particle geometry," Nano Lett. **15**(1), 530–534 (2015).
45. H. Husu, R. Siikanen, J. Mäkitalo, J. Lehtolahti, J. Laukkanen, M. Kuittinen, and M. Kauranen, "Metamaterials with tailored nonlinear optical response," Nano Lett. **12**(2), 673–677 (2012).
46. M. S. Bin-Alam, O. Reshef, R. N. Ahmad, J. Upham, M. J. Huttunen, K. Dolgaleva, and R. W. Boyd, "Cross-polarized surface lattice resonances in a rectangular lattice plasmonic metasurface," arXiv preprint 2111.02472 (2021).
47. W. N. Herman and L. M. Hayden, "Maker fringes revisited: second-harmonic generation from birefringent or absorbing materials," J. Opt. Soc. Am. B **12**(3), 416–427 (1995).
48. L. Alloatti, C. Kieninger, A. Froelich, M. Lauermann, T. Frenzel, K. Köhnle, W. Freude, J. Leuthold, M. Wegener, and C. Koos, "Second-order nonlinear optical metamaterials: Abc-type nanolaminates," Appl. Phys. Lett. **107**(12), 121903 (2015).
49. B. Metzger, L. Gui, J. Fuchs, D. Floess, M. Hentschel, and H. Giessen, "Strong Enhancement of Second Harmonic Emission by Plasmonic Resonances at the Second Harmonic Wavelength," Nano Lett. **15**(6), 3917–3922 (2015).
50. B. Metzger, M. Hentschel, and H. Giessen, "Probing the Near-Field of Second-Harmonic Light around Plasmonic Nanoantennas," Nano Lett. **17**(3), 1931–1937 (2017).
51. C. Langhammer, M. Schwind, B. Kasemo, and I. Zoric, "Localized surface plasmon resonances in aluminum nanodisks," Nano Lett. **8**(5), 1461–1471 (2008).

Optics EXPRESS

52. E. Benichou, G. Bachelier, C. Jonin, P. F. Brevet, and C. B. Lyon, "Multipolar Contributions of the Second Harmonic Generation from Silver and Gold Nanoparticles," J. Phys. Chem. C **111**(26), 9044–9048 (2007).
53. T. Stolt, J. Kim, S. Héron, A. Vesala, Y. Yang, J. Mun, M. Kim, M. J. Huttunen, R. Czaplicki, M. Kauranen, J. Rho, and P. Genevet, "Backward phase-matched second-harmonic generation from stacked metasurfaces," Phys. Rev. Lett. **126**(3), 033901 (2021).
54. T. Stolt and M. J. Huttunen, "Broadband frequency conversion of ultrashort pulses using high-q metasurface cavities," arXiv preprint 2110.13486 (2021).
55. M. J. Huttunen, P. Rasekh, R. W. Boyd, and K. Dolgaleva, "Using surface lattice resonances to engineer nonlinear optical processes in metal nanoparticle arrays," Phys. Rev. A **97**(5), 053817 (2018).